Contrib Mineral Petrol (2007) 154:75–90
DOI 10.1007/s00410-007-0180-1

ORIGINAL PAPER

Fluid–rock interaction at a carbonatite-gneiss contact, Alnö, Sweden

A. Skelton · J. Hode Vuorinen · F. Arghe · A. Fallick

Received: 19 August 2006 / Accepted: 11 January 2007 / Published online: 16 February 2007
© Springer-Verlag 2007

Abstract We evaluate balanced metasomatic reactions and model coupled reactive and isotopic transport at a carbonatite-gneiss contact at Alnö, Sweden. We interpret structurally channelled fluid flow along the carbonatite-gneiss contact at ~640°C. This caused (1) metasomatism of the gneiss, by the reaction: biotite + quartz + oligoclase + K_2O + Na_2O ± CaO± MgO ± FeO = albite + K-feldspar + arfvedsonite + aegirene-augite + H_2O + SiO_2, (2) metasomatism of carbonatite by the reaction: calcite + SiO_2 = wollastonite + CO_2, and (3) isotopic homogenization of the metasomatised region. We suggest that reactive weakening caused the metasomatised region to widen and that the metasomatic reactions are chemically (and possibly mechanically) coupled. Spatial separation of reaction and isotope fronts in the carbonatite conforms to a chromatographic model which assumes local calcite–fluid equilibrium, yields a timescale of 10^2–10^4 years for fluid–rock interaction and confirms that chemical transport towards the carbonatite interior was mainly by diffusion. We conclude that most silicate phases present in the studied carbonatite were acquired by corrosion and assimilation of ijolite, as a reactive by-product of this process and by metasomatism. The carbonatite was thus a relatively pure calcite–H_2O–CO_2–salt melt or fluid.

Keywords Carbonatite · Fluid flow · Metasomatism · Alnö

Communicated by J. Hoefs.

A. Skelton (✉) · J. Hode Vuorinen · F. Arghe
Department of Geology and Geochemistry,
Stockholm University, 10691 Stockholm, Sweden
e-mail: alasdair.skelton@geo.su.se

A. Fallick
Scottish Universities Environmental Research Centre,
Rankine Avenue, Scottish Enterprise Technology Park,
East Kilbride G750QF, Scotland

Introduction

Fluid–rock interaction associated with the emplacement of carbonatite or alkaline magmas can cause a wide range of mineral reactions, which affect both the wall rock of the intrusive complex and the complex itself (e.g., Brögger 1921; Eckermann 1948; Kresten and Morogan 1986; Morogan and Woolley 1988; Kramm 1994; Sindern and Kramm 2000). These reactions typically require the addition or removal of components, which enter or exit the system, transported by a fluid. For example, fenitisation, as defined by Brögger (1921) to describe the transformation of granitic gneiss to syenite at Fen, Norway, requires the removal of silica and addition of alkalis. Several petrological and geochemical studies infer the transferral of a wider range of components. These include the transformation of migmatitic gneiss to ijolites and nepheline syenites on Alnö, Sweden, proposed by Eckermann (1948), ijolite formation at Iivaara, Finland, proposed by Kramm (1994), and formation of the ''contact fenites'' of Morogan and Woolley (1988) on Alnö. The extensive component mobility inferred by these studies renders the distinction between mineral assemblages that are of truly igneous origin and those that partly or wholly represent the product of fluid–rock interaction problematic. This, in turn, limits our

ability to understand the petrogenetic origin, evolution and significance of carbonatite and alkaline magmas.

In this paper, we evaluate balanced metasomatic reactions and inter-mineral isotopic fractionation factors and we use a chromatographic approach to model coupled reactive and isotopic transport at a carbonatite-gneiss contact, which crops out at the Smedsgården quarry on Alnö, Sweden (Fig. 1). We attempt to define and ''remove'' the fluid–rock interaction ''overprint'' to reveal those petrological and isotopic characteristics that are of igneous origin.

Geological background

The Precambrian (584 ± 13 Ma; Andersen 1996) Alnö complex consists of nepheline syenites, ijolites and carbonatites (Eckermann 1948; Kresten 1979, 1980). Carbonatites occur as dykes, varying in width from a few centimetres to several tens of metres. The widest dykes are traceable for several tens of meters along strike, while smaller dykes usually taper off within a couple of meters, becoming thin and vein-like. The 4 km^2 complex is hosted by migmatitic gneisses.

Hode Vuorinen et al. (2005) demonstrated the genetic association of the alkaline igneous rocks on Alnö, arguing that the nepheline syenites are produced by differentiation of layered ijolite series rocks. How the alkaline igneous rocks and carbonatites, cropping out on Alnö, might be petrogenetically related remains controversial (e.g., Morogan and Woolley 1988; Hode Vuorinen and Skelton 2004; Hode Vuorinen et al. 2005). Despite this controversy, most authors agree that a common origin is required to explain the spatial association of carbonatites and alkaline igneous rocks. Cross-cutting relationships further indicate that the carbonatite intrusion post-dated emplacement of the alkaline silicate suite on Alnö.

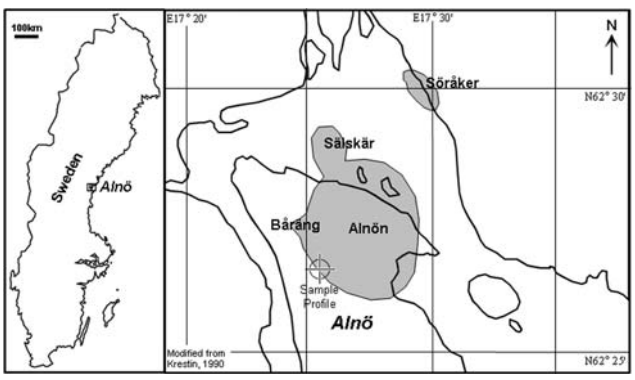

Fig. 1 Location map. The island Alnö is located near the town of Sundsvall in east-central Sweden. The four igneous centers of the complex: Söråker, Sälskar, Båräng and Alnön are shown (*shaded*). The sample profile was taken at the Smedsgården quarry which is situated at the southwestern edge of the Alnö intrusion

Fluid–rock interaction on Alnö was first described by Eckermann (1948). He used the term fenitisation to describe metasomatism of the migmatitic gneiss by fluids derived from the carbonatite dykes. He proposed that all other rocks (including those now thought to be alkaline igneous rocks), were products of metasomatism. Morogan and Woolley (1988) provided a thorough and rigorous reappraisal of fluid–rock interaction on Alnö, concurring with other workers (e.g., Kresten 1979, 1980), that the alkaline rocks were igneous and that most evidence of fluid–rock interaction was found within a 500–600 m wide aureole surrounding the complex. Morogan and Woolley (1988) used the term fenitisation to describe a range of mineralogical and textural changes in the migmatitic gneiss. These include (1) granulation, undulatory extinction and the progressive disappearance of quartz, (2) turbidity in feldspars, their overgrowth and replacement by albite and reddening due to hematite inclusions, (3) recrystallisation of biotite to a fine-grained aggregate with K-feldspar and hematite, and (4) growth of arfvedsonite and aegirine–augite. They used the term ''contact fenite'' to describe rocks, which they interpreted to be of metasomatic origin and which occur adjacent to carbonatite dykes and contain nepheline + diopside + calcite ± wollastonite ± Ti-andradite.

This study was conducted at Smedsgården (Fig. 1), where a partly altered migmatitic gneiss is separated from a carbonatite dyke by a 1.4 m wide shear zone and a zone containing nepheline + diopside + calcite ± wollastonite ± Ti-andradite (Fig. 2). Because the focus of this study is on the petrological and isotopic changes caused by fluid–rock interaction and because of the ambiguity and controversy surrounding terms such as ''fenitisation'' and ''contact fenite'', we will hereafter refer to all such changes, which are caused by fluid–rock interaction as ''metasomatism''.

Smedsgården

The quarry at Smedsgården provides an ideal natural laboratory to study fluid–rock interaction associated with carbonatite emplacement, with 52 m of continuous outcrop (measured perpendicular to the strike of the carbonatite dyke) consisting of (from SW to NE) ca. 25 m of migmatitic gneiss, a 1.4 m wide shear zone, 7 m of nepheline + diopside + calcite ± wollastonite ± Ti-andradite rock and ca. 18 m of carbonatite (Fig. 2).

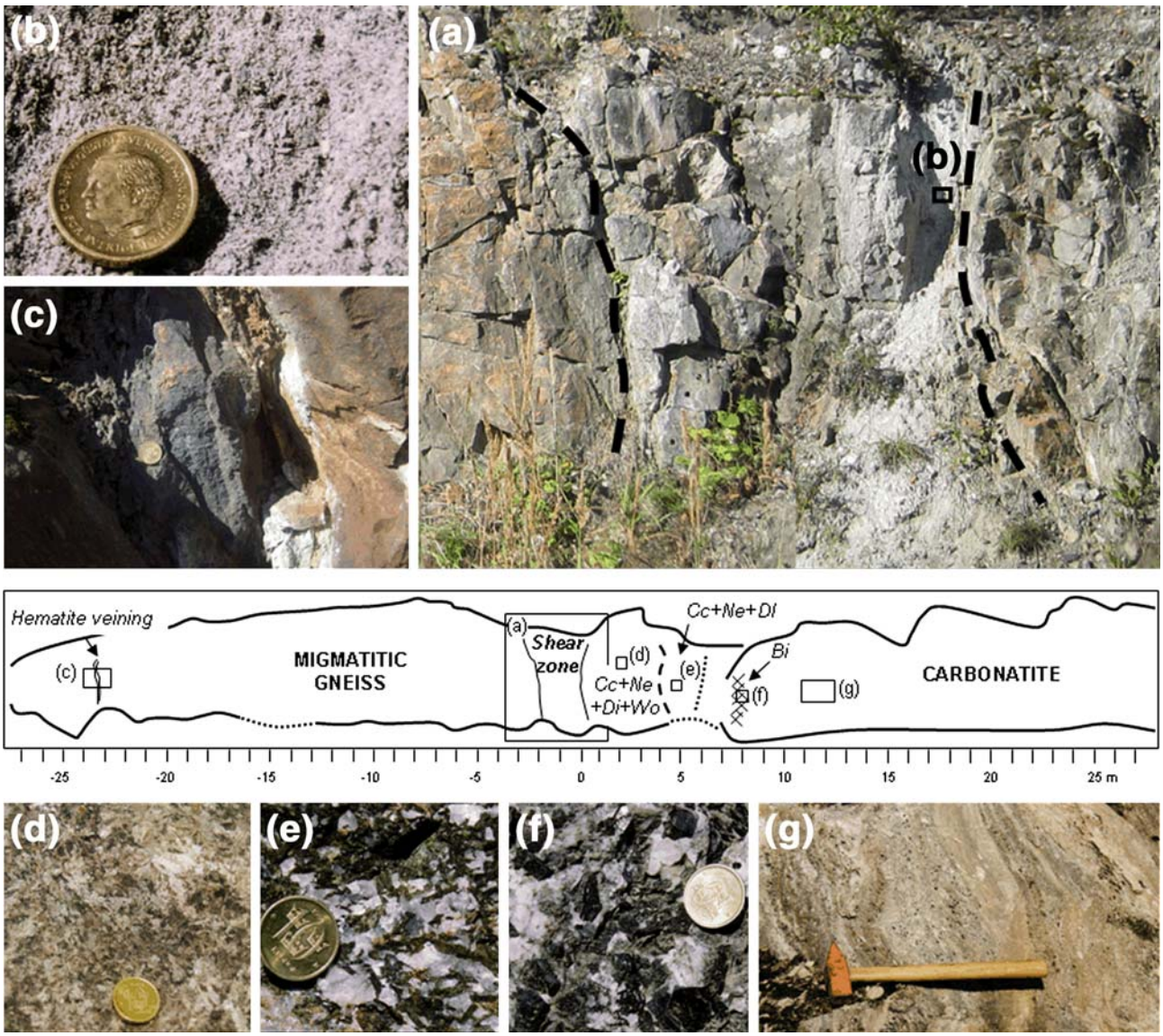

Fig. 2 Studied profile at Smedsgården, Alnö, showing **a** an overview of the ~1. 5 m wide shear zone and close ups of **b** fragmented wollastonite in the shear zone, **c** the zone of hematite veining, **d** the calcite + nepheline + diopside + wollastonite rock, **e** the calcite + nepheline + diopside rock, **f** euhedral biotite and **g** flow banding in the carbonatite

The gneiss at Smedsgården is partly metasomatised. Where least metasomatised, it contains oligoclase (An_{24}), quartz, and biotite, which is similar to gneiss collected at distances >1 km from the complex. Metasomatism of the gneiss occurs both adjacent to the shear zone and surrounding a region with extensive hematite veining, located 23.6 m SW of the shear zone (Fig. 2). Adjacent to the shear zone, metasomatism is characterized by the breakdown of biotite to a fine-grained aggregate with K-feldspar and hematite, and the subsequent nucleation and growth of granules and/or laths of aegirine-augite and/or arfvedsonite (Fig. 3a). The distribution of these reaction products on a dm-scale is patchy, with highly metasomatised and weakly metasomatised regions occurring in close proximity. This patchy distribution may, in part, reflect preferential nucleation of the product minerals along fractures (Fig. 3b). Surrounding the region of hematite veining, metasomatism is characterized by the reddening of feldspar. In thin section, oligoclase is overgrown by albite in this region (Fig. 3c). The reddening is probably caused by hematite grains occupying sub-optical pores, produced during the dissolution of oligoclase and precipitation of albite (Parsons, personal communication).

The shear zone consists of a fine-grained crumbly matrix of fragmented wollastonite grains (Fig. 2). Sheared m-scale lens-shaped blocks of metasomatised

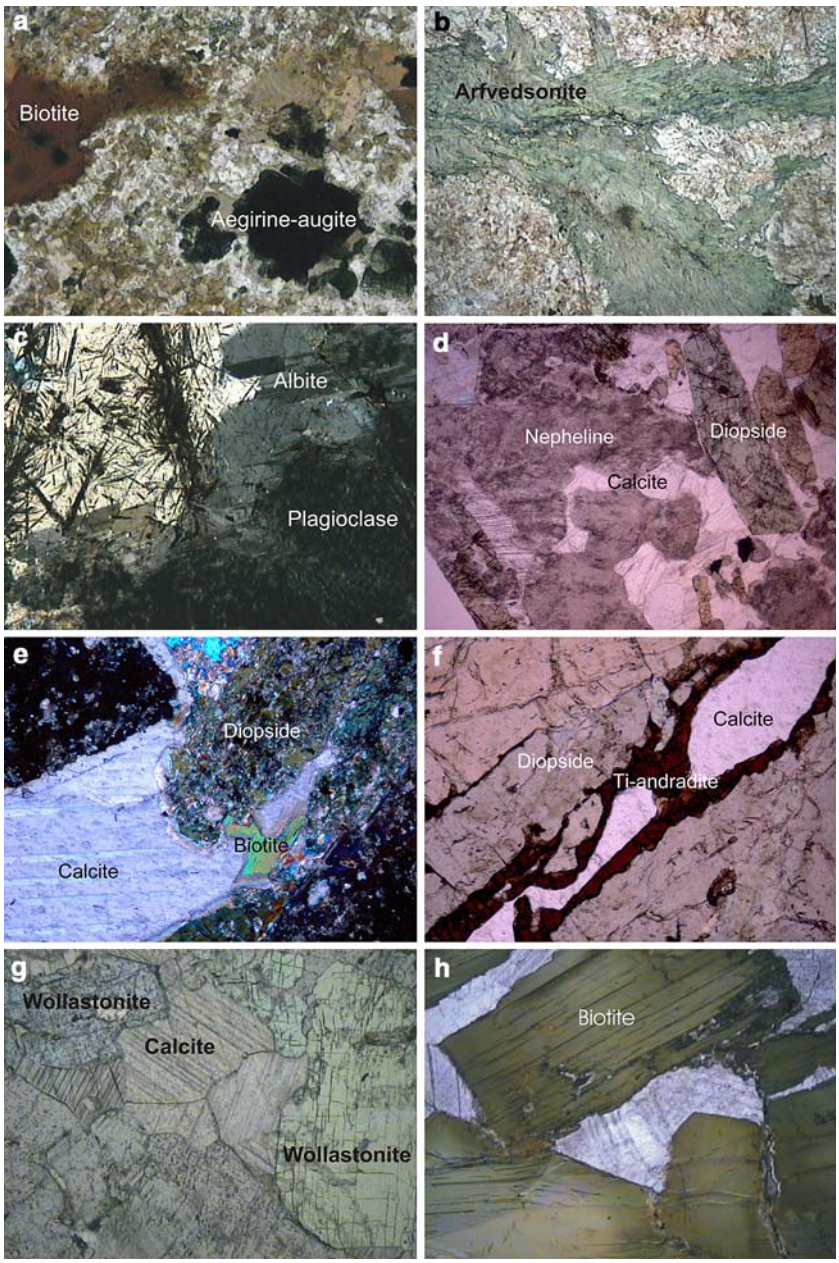

Fig. 3 Photomicrographs from the Smedsgården profile showing **a** the reaction texture: biotite → aegirine-augite (image size: ca. 1.5 × 1.0 mm, PPL), **b** growth of arfvedsonite along fractures (image size ca. 5 × 3 mm, PPL), **c** the reaction texture: oligoclase → albite. (image size: ca. 1.5 × 1.0 mm, XP), **d** corrosion of nepheline with interstitial calcite (image size: ca. 1.5 × 1.0 mm, PPL), **e** corrosion of diopside (image size ca. 5 × 3 mm, XP), **f** boundary film of Ti-andradite along calcite–diopside grain boundary (image size ca. 5 × 3 mm, PPL), **g** euhedral wollastonite in carbonatite (image size: ca. 5 × 3 mm, PPL) and **h** biotite in carbonatite (image size: ca. 5 × 3 mm, PPL). XP = crossed polars, PPL = plain polarised light

migmatitic gneiss and the adjacent nepheline + diopside + calcite ± wollastonite ± Ti-andradite rock are supported within the fragmented wollastonite matrix. Shearing of these blocks is parallel to the strike of the carbonatite dyke (Fig. 2a). However, wollastonite crystals show little or no preferential alignment (Fig. 2b). This suggests that little or no displacement occurred along the shear zone after wollastonite formed.

The region of extensive hematite veining varies in width from 5 to 20 cm and is characterised by anastamosing veins and patches of hematite. Hematite also occurs disseminated throughout the surrounding migmatitic gneiss.

The nepheline + diopside + calcite ± wollastonite ± Ti-andradite rock occurs immediately northeast of the shear zone (Fig. 2). Wollastonite is only present within the part of this zone which is closest to the shear zone. Nepheline and diopside crystals are partly corroded (Fig. 3d, e). Calcite is interstitial. Ti-andradite occurs both as euhedral crystals and as boundary films along diopside-calcite grain boundaries (Fig. 3f). Wollastonite occurs as 1–2 cm long euhedral crystals (Fig. 3g). The origin of this rock is controversial. Morogan and Woolley (1988) classify it as a contact fenite produced by metasomatism of the gneiss. Hode Vuorinen and Skelton (2004) present field and textural

evidence which suggests that much of the nepheline and diopside in the carbonatite dykes at Smedsgården and elsewhere on Alnö were derived from ijolites along the intrusion pathway by (1) infiltration along grain-boundaries by the carbonatite liquid, (2) reaction (or corrosion), (3) mechanical fragmentation and (4) assimilation. Hode Vuorinen and Skelton (2004) note that phlogopite is expected as a by-product of this reaction. We adopt their interpretation and suggest that this unit represents carbonatite containing (and infiltrating) variably assimilated ijolite. This interpretation is supported by (1) the interstitial nature of calcite and the corroded appearance of nepheline and diopside in this rock (Fig. 3d, e), and (2) nepheline + diopside ± Ti-andradite fragments and euhedral phlogopite in the carbonatite dyke (Fig. 3h). Hode Vuorinen and Skelton (2004) offer no explanation for the high modal content of wollastonite (which we have observed in no more than trace quantities elsewhere on Alnö) near the shear zone. Based on (1) its euhedral form and the lack of evidence of its corrosion by the carbonatite liquid (Fig. 3g) and (2) its spatial association with the shear zone, which is a likely fluid channel, we adopt and will later test (by comparison with stable isotope data to confirm the direction of fluid flow) the hypothesis that wollastonite is produced by metasomatism of the carbonatite, rather than by igneous crystallization or metasomatism of the gneiss as suggested in some previous studies (Bailey 1974; Church and Jones 1995; Morogan and Woolley 1988). It is unclear whether Ti-andradite is (partly) assimilated from ijolite (similar to nepheline and diopside), a by-product of the assimilation reaction (similar to phlogopite), or a product mineral formed by metasomatism of the carbonatite (similar to wollastonite).

Finally, sensu stricto carbonatite (which contains >50 modal % calcite) occurs further to the northeast (Fig. 2). It is strongly banded on a dm scale (Fig. 2), with preferential alignment and elongation of calcite crystals parallel to this banding. Nepheline, diopside and Ti-andradite occur as isolated grains, which are generally corroded in appearance, or as partly corroded blocks of nepheline + diopside ± Ti-andradite (Fig. 2). Phlogopite occurs in discrete dm-wide zones as 1–2 cm diameter euhedral crystals (Fig. 3h).

Petrological evidence of fluid–rock interaction

In this section, we attempt to balance reactions to explain observed modal changes (estimated by point counting) and textural evidence of reaction progress and component mobility in (1) the gneiss (SW of the shear zone) and (2) the carbonatite (NE of the shear zone).

Metasomatism of the migmatitic gneiss

Mineral modes of the metasomatised migmatitic gneiss were determined by standard point-counting methods. These data are listed in Table 1 and plotted as a function of distance from the shear zone in Fig. 4. About 1,000 points were counted on each sample, which yields a 2σ error of $2\sqrt{x_{j(\mathrm{or}\,k)}\left(100 - x_{j(\mathrm{or}\,k)}\right)/1000}$ modal %, where x_j (or x_k) is the modal % of reactant mineral j (or product mineral k) (van der Plas and Tobi 1965). Feldspar identifications were confirmed by electron microprobe analysis of ''end-member'' samples (types I and II, see below). Based on this profile, we delineate the following two mineral assemblage types:

Type I: Unaltered (or weakly metasomatised) gneiss, containing 14.4 ± 2.2 % biotite, 36.1 ± 3.0 % quartz, 27.9 ± 2.8 % oligoclase (An_{24}) and 21.6 ± 2.2 %, K-feldspar.

Type II: Strongly metasomatised gneiss, containing 5.0 ± 1.4% aegirine-augite, 19.7 ± 2.5% arfvedsonite, 10.5 ± 1.9% albite, 63.7 ± 3.0% K-feldspar. Biotite and quartz are absent. The modal abundances of aegirine-augite and arfvedsonite are highly variable on a length scale of 0.1–1 m, but vary more systematically on a length scale of 1–10 m.

The type II gneiss was observed occupying a 2–3 m wide zone immediately adjacent to the shear zone and a 3–5 m wide zone NE of the region of hematite veining at $z = 23.6$ m. These zones were separated from type I gneiss by variably broadened reaction fronts, with coexisting biotite, quartz, aegirine–augite, arfvedsonite, oligoclase, albite and K-feldspar. Based on the above modal data, we can construct the metasomatic reaction (volumetric units):

$$\begin{aligned} &14.4\,(\pm 2.2)\ \text{biotite} + 36.1\,(\pm 3.0)\ \text{quartz} \\ &\quad + 27.9\,(\pm 2.8)\ \text{oligoclase} = 10.5\,(\pm 1.9)\ \text{albite} \\ &\quad + 42.1\,(\pm 3.1)\ \text{K-feldspar} + 19.7\,(\pm 2.5)\ \text{arfvedsonite} \\ &\quad + 5.0\,(\pm 1.4)\ \text{aegirene-augite} \pm \text{mobile components} \end{aligned} \tag{1a}$$

The forwards progress of this metasomatic reaction is supported by the following textural evidence:

- Biotite is replaced by aegirene-augite (Fig. 3a.)
- Arfvedsonite is formed as vein fill (Fig. 3b.)
- Oligoclase is replaced by albite (Fig. 3c.)

Table 1 Stable isotope and modal (point counting) data

z (m)	Stable isotope data				Point counting data										
	$\delta^{18}O_{SMOW}$-feldspar	$\delta^{18}O_{SMOW}$-calcite	$\delta^{18}O_{SMOW}$-diopside	$\delta^{13}C_{PDB}$-calcite	Bi	Qz	Fsp	Arf	Aeg	Wo	Cc	Ne	Di	Gt	Or
–30	10.26				14.4 ± 2.2	36.1 ± 3.0	49.5 ± 3.2 Plag: 27.9 ± 2.8 *K*-fsp: 21.6 ± 2.6								
–26.8	6.9														
–26.3	8.16				11.0 ± 2.0	16.7 ± 2.4	52.5 ± 3.2								
–23.6	6.23				25.0 ± 2.7	20.0 ± 2.5	37.0 ± 3.1		16.0 ± 2.3						
–21.5	6.94					0.8 ± 0.5	72.3 ± 2.8								
–19	8.01					1.5 ± 0.8	77.8 ± 2.6								
–16.8	7.49				18.0 ± 2.4	1.0 ± 0.6	29.7 ± 2.9								
–14.2	8.03														
–11.7					27.7 ± 2.8	5.3 ± 1.4	49.8 ± 3.2	7.2 ± 1.6	10.1 ± 1.9						
–10	8.84				38.1 ± 3.1	5.8 ± 1.5	50.2 ± 3.2	4.2 ± 1.3	0.7 ± 0.5						
–9.5	9.3														
–9	9.7														
–8.5	8.8				27.4 ± 2.8	8.3 ± 1.7	51.7 ± 3.2	5.1 ± 1.4	5.5 ± 1.4						
–8	7.8														
–7.6	9.55				29.8 ± 2.9	17.5 ± 2.4	35.5 ± 3.0	14.0 ± 2.2	2.2 ± 0.9						
–7.1	9.3														
–6.4	8.8														
–5.8	9.1														
–5.3	8.84				21.6 ± 2.6	20.8 ± 2.6	54.2 ± 3.2	1.2 ± 0.7	1.2 ± 0.7						
–4.4	9.1														
–3.8	8.38				15.9 ± 2.3	14.6 ± 2.2	58.4 ± 3.1	4.6 ± 1.3	2.4 ± 1.0						
–2.9	8.07				9.9 ± 1.9	7.5 ± 1.7	77.5 ± 2.6	3.5 ± 1.2	0.6 ± 0.5						
–2.5	8.5														
–1.6	8.35					0.2 ± 0.3	74.0 ± 2.8 *K*-fsp: 63.7 ± 3.0 *Ab*: 10.3 ±1.9	19.7 ± 2.5	5.0 ± 1.4						
–1.4	8.2														
0.4		8.46	5.58	–4.34						31.8 ± 4.2	5.0 ± 1.9	26.8 ± 4.0	34.0 ± 4.2	1.2 ± 1.0	1.0 ± 0.9
0.7			5.93							56.8 ± 4.4	5.0 ±1.9	12.4 ± 2.9	16.2 ± 3.3	7.4 ± 2.3	1.6 ± 1.1
1.0			5.78							34.8 ± 4.3	9.6 ± 2.6	21.8 ± 3.7	31.6 ± 4.2	0.8 ± 0.8	1.4 ± 1.1
1.4		8.35		–5.03						20 ± 3.6	8.2 ± 2.5	46.4 ± 4.5	21.0 ± 3.6	4.4 ± 1.8	
1.7			6.14							24.8 ± 3.9	6.2 ± 2.2	14.4 ± 3.1	50.6 ± 4.5	0.2 ± 0.4	3.8 ± 1.7
2.1		8.21	5.72	–5.73						41.8 ± 4.4	18.4 ± 3.5	20.2 ± 3.6	16.4 ± 3.3	1.4 ± 1.1	1.8 ± 1.2
2.3			5.6							53.2 ± 4.5	3.0 ± 1.5	32 ± 4.2	6.2 ± 2.2	3.6 ± 1.7	1.8 ± 1.2
2.5		8.52		–5.53						27.6 ± 4.0	13.0 ± 3.0	35.4 ± 4.3	20.6 ± 3.6	0.6 ± 0.7	1.4 ± 1.1
2.8		8.26	5.77	–5.21						41.6 ± 4.4	5.0 ± 1.9	26.0 ± 3.9	19.4 ± 3.5	3.6 ± 1.7	4.4 ± 1.8
3.1			6.36							32.2 ± 4.2	8.6 ± 2.5	25.2 ± 3.9	25.2 ± 3.9	6.8 ± 2.3	1.0 ± 0.9
3.5		8.41	6.03	–4.59						9.8 ± 2.7	5.8 ± 2.1	24.8 ± 3.9	52.4 ± 4.5	7.2 ± 2.3	
3.8										0.2 ± 0.4	25.4 ± 3.9	26.0 ± 3.9	40.2 ± 4.4	4.0 ± 1.8	4.2 ± 1.8
4.2		8.20	6.07	–7.09						21.0 ± 3.6	15.2 ± 3.2	15.6 ± 3.2	34.4 ± 4.2	5.2 ± 2.0	7.6 ± 2.4
4.6		8.32	6	–4.86						17.8 ± 3.4	11.6 ± 2.9	20.2 ± 3.6	26.8 ± 4.0	21.6 ± 3.7	2.0 ± 1.3
4.9		8.30	6.51	–5.10											
5.3		7.77	5.46	–4.83						2.8 ± 1.5	7.6 ± 2.4	41.0 ± 4.4	29.4 ± 4.1	17.8 ± 3.4	0.6 ± 0.7
5.6		8.72	6.265	–4.91						0.4 ± 0.6	21.2 ± 3.7	32.2 ± 4.2	35.2 ± 4.3	4.4 ± 1.8	5.2 ± 2.0
6.0		7.43	5.88	–4.48						0.2 ± 0.4	27.2 ± 4.0	1.2 ± 1.0	66.0 ± 4.2	0.8 ± 0.8	1.8 ± 1.2

Table 1 continued

z (m)	Stable isotope data				Point counting data										
	$\delta^{18}O_{SMOW}$-feldspar	$\delta^{18}O_{SMOW}$-calcite	$\delta^{18}O_{SMOW}$-diopside	$\delta^{13}C_{PDB}$-calcite	Bi	Qz	Fsp	Arf	Aeg	Wo	Cc	Ne	Di	Gt	Or
6.5		7.43	5.17	–4.46							49.8 ± 4.5	9.6 ± 2.6	36.6 ± 4.3	0.8 ± 0.8	2.8 ± 1.5
7.5		7.26		–4.37	4.2 ± 1.3						72.1 ± 4.0		14.0 ± 3.1		
8.2		7.17		–4.35											
8.9		7.28		–4.40	7.5 ± 1.7						85.4 ± 3.2				0.1 ± 0.3
9.6		7.16		–4.30	9.5 ± 1.9						79.7 ± 3.6				
10.3		7.29		–4.34	5.2 ± 1.4						84.2 ± 3.3				
11.0		8.20		–4.05											
11.8		7.25		–4.41											
13.7		7.14		–4.42											
15.8		7.40		–4.46	12.2 ± 2.1						84.1 ± 3.3		0.1 ± 0.3		
18.4		7.27		–4.40	8.4 ± 1.8						80.5 ± 3.5				
20.4		7.51		–4.47											
21.4		7.49		–4.99											
22.6		7.41		–4.58											

Stable isotope data ($\delta^{18}O_{SMOW}$ and ($\delta^{13}C_{PDB}$) for feldspar, diopside and calcite mineral separates. Precision (1σ) is ±0.1‰. Modal (point counting) data for biotite (Bi), quartz (Qz), feldspar (Fsp), arfvedsonite (Arf), aegirene-augite (Aeg), wollastonite (Wo), calcite (Cc), nepheline (Ne), diopside (Di), garnet (Gt) and orthoclase (Or). Modes of plagioclase (Plag), K-feldspar (K-fsp) and albite (Ab) were estimated for samples at z = –30 and –1.6 m

In the following analysis, we calculated the metasomatic addition (positive) or subtraction (negative) of components i (n_i) per unit volume of reactant gneiss, caused by the forwards progress of reaction (1). This is expressed in mol m^{-3} by the equation: $n_i = \sum n_k\ [i]_k - \sum n_j\ [i]_j$. In this equation, n_j and n_k represent the number of moles of reactant minerals j (biotite, quartz and oligoclase) and product minerals k (albite, K-feldspar, arfvedsonite and aegirene–augite) per unit volume of reactant gneiss. For each mineral, n_j (or n_k) was evaluated from its volumetric mode [x_j (or x_k)], molar weight (calculated for the mineral compositions given in Table 2) and density. n_j and n_k are expressed in units of mol m^{-3}. $[i]_j$ and $[i]_k$ represent the molar proportion of component i in reactant minerals j and product minerals k, respectively. For an initial assumption of constant volume (cf. Gresens 1967), we obtained the metasomatic reaction, expressed in mol m^{-3}:

$$\begin{aligned}
&480\,(\pm74)\ \text{biotite} + 16245\,(\pm1367)\ \text{quartz}\\
&\quad + 2731\,(\pm278)\ \text{oligoclase} + 1366\,(\pm67)\ K_2O\\
&\quad + 310\,(\pm106)\ Na_2O + 462\,(\pm140)\ CaO\\
&\quad + 2158\,(\pm281)\ MgO + 511\,(\pm102)\ FeO\\
&\quad + 130\,(\pm39)\ Al_2O_3 = 1052(\pm193)\ \text{albite}\\
&\quad + 4033\,(\pm295)\ \text{K-feldspar} + 853\,(\pm108)\ \text{arfvedsonite}\\
&\quad + 787\,(\pm216)\ \text{aegirene-augite} + 2952\,(\pm200)\ SiO_2\\
&\quad + 49\,(\pm8)\ TiO_2 + 106\,(\pm40)\ H_2O \qquad (1b)
\end{aligned}$$

The mobility of Al_2O_3 is likely to be low, compared with most other components, particularly in alkaline metasomatic fluids (Sokolova and Khodakovskiy 1977). We therefore recast this reaction with $n_{Al_2O_3}$ set to zero by adjusting the volume change for the reaction. For a total volume reduction of 3.9%, we obtained:

$$\begin{aligned}
&480\,(\pm74)\ \text{biotite} + 16245\,(\pm1367)\ \text{quartz}\\
&\quad + 2731\,(\pm278)\ \text{oligoclase} + 1275\,(\pm66)\ K_2O\\
&\quad + 241\,(\pm101)\ Na_2O + 406\,(\pm135)\ CaO\\
&\quad + 1983\,(\pm272) MgO + 435\,(\pm96)\ FeO +\\
&= 1000\,(\pm189)\ \text{albite} + 3832\,(\pm293)\ \text{K-feldspar}\\
&\quad + 810\,(\pm106)\ \text{arfvedsonite}\\
&\quad + 748\,(\pm211)\text{aegirene-augite} + 4120\,(\pm155)\ SiO_2\\
&\quad + 53\,(\pm8)\ TiO_2 + 149\,(\pm42)\ H_2O \qquad (1c)
\end{aligned}$$

This reaction consumes 78.4 ± 2.6 volume % of the reactant gneiss, the remainder of which is mainly excess K-feldspar. Significant quantities of K_2O, Na_2O, CaO, MgO and FeO are consumed and significant quantities of SiO_2 and H_2O are released by

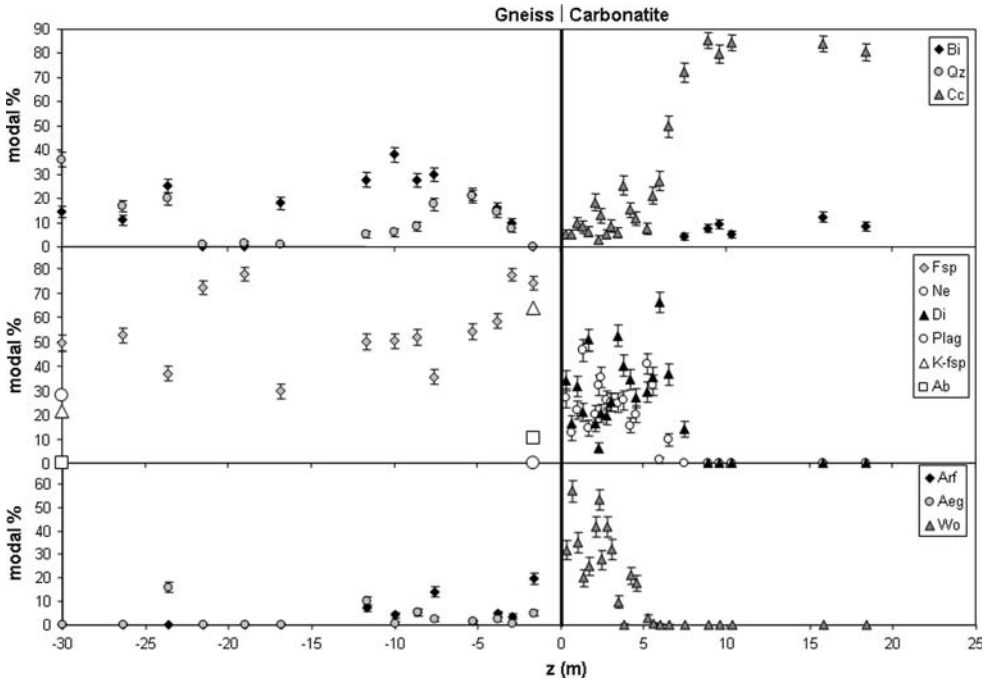

Fig. 4 Profile across the outcrop at Smedsgården showing modal data estimated by point counting (1,000 points/thin section)

Table 2 Compositional data

Weight%	Gneiss (type I)		Gneiss (type II)				Carbonatite (type II)	
	K-fsp	Plag	Bi	Aeg	Arf	Ab	K-fsp	Wo
SiO_2	64.17	62.08	35.16	52.23	53.72	68.19	64.37	50.92
TiO_2	0.01	0.00	2.16	0.53	0.60	0.01	0.02	0.03
Al_2O_3	18.70	23.57	18.19	0.64	1.61	19.06	17.74	0.01
Fe_2O_3	0.03	0.02	0.00	14.48	0.00	0.53	0.68	0.00
FeO	0.00	0.00	16.45	4.84	9.70	0.00	0.00	0.57
MnO	0.00	0.02	0.35	0.62	0.54	0.01	0.01	0.31
MgO	0.00	0.00	12.23	6.75	17.23	0.00	0.01	0.14
CaO	0.29	5.07	0.01	14.08	4.82	0.01	0.01	47.81
Na_2O	1.80	8.91	0.33	5.91	6.88	11.75	1.17	0.01
K_2O	14.33	0.22	9.63	0.01	1.60	0.18	15.25	0.00
Cr_2O_3	0.00	0.01	0.06	0.07	0.02	0.01	0.01	0.01
Total	99.35	99.90	94.57	100.16	96.71	99.75	99.27	99.82
Average of analyses (*n*)	2	5	23	41	8	6	5	5

Compositional data for K-feldspar (K-fsp), oligoclase (Plag), biotite (Bi), aegirene-augite (Aeg), arfvedsonite (Arf), albite (Ab) and wollastonite (Wo) from the gneiss (types I and II) and carbonatite (type II). These data were determined by electron microprobe analysis at the Department of Earth Sciences, Uppsala University, Sweden

the metasomatic reaction. Reaction (1) is similar to fenitisation, as defined by Brögger (1921), in that alkalis are added and silica is removed. Reaction (1) further predicts the addition of CaO, MgO and FeO. However, we cannot exclude that this is partly an artifact of the observed variability in the modes of arfvedsonite and aegirene-augite.

The chemical changes predicted by reaction (1c) are similar to those reported by Verschure and Maijer (2005) for ''fenitisation'' of the Fen ring complex, South Norway. These authors reported the release of silica and addition of alkalis, CaO, MgO and Fe_2O_3 during fenitisation. They concluded that the first (high T) phase of fenitisation, which affected the Fen ring complex, caused dehydration.

We were unable to find petrographic evidence for the volume loss inferred by reaction (1c), but we note that volume loss could have been accommodated within the shear zone and/or partly compensated by volume gain in the carbonatite (see below).

Metasomatism of the carbonatite

The modal mineralogy of the sensu stricto carbonatite and the carbonatite containing/infiltrating variably assimilated ijolite was estimated by point-counting. These data are listed in Table 1 and plotted as a function of distance from the shear zone in Fig. 4. Based on this profile, we delineate the following three mineral assemblage types:

Type Ia: >80% calcite and ~10% biotite.
Type Ib: >50% calcite and <50% diopside + nepheline.
Type II. 36 ± 12% wollastonite, <10% calcite, and ~50% diopside + nepheline.

The type II assemblage occupies a 3 m wide zone immediately adjacent to the shear zone. If our hypothesis is correct and wollastonite is produced by metasomatism of the carbonatite, we can conclude that the type I and II assemblages are separated by a 3 m wide reaction front and that the type II assemblage represents a metasomatised carbonatite containing/infiltrating variably assimilated ijolite. We can construct the metasomatic reaction:

$$\text{calcite} = \text{wollastonite} \pm \text{mobile components} \quad (2a)$$

For an initial assumption of constant volume (cf. Gresens 1967) and for the production of 36 ± 12 volume% wollastonite, we obtained the metasomatic reaction (for pure end-member compositions), expressed in mol m^{-3}:

$$\begin{aligned} &10125\,(\pm827)\,\text{calcite} + 9698\,(\pm792)\,SiO_2 \\ &\quad = 9698\,(\pm792)\,\text{wollastonite} + 427\,(\pm35)\,CaO \\ &\qquad + 10125\,(\pm827)\,CO_2 \end{aligned} \quad (2b)$$

We consider it unlikely that both CaO and CO_2 are released by this reaction and we therefore recast this reaction with n_{CaO} set to zero by adjusting the volume change for the reaction. For a total volume gain of 1.6%, we obtained:

$$\begin{aligned} &9698\,(\pm819)\,\text{calcite} + 9698\,(\pm792)\,SiO_2 \\ &\quad = 9698\,(\pm792)\,\text{wollastonite} + 9698\,(\pm819)\,CO_2 \end{aligned} \quad (2c)$$

This reaction consumes calcite and produces wollastonite by metasomatic addition of silica. Lack of modal variance of nepheline or diopside across the reaction zone confirms that these minerals are not involved in the reaction. The calcite (+wollastonite) part of the rock (which is involved in the reaction) matches the definition of skarn by Einaudi and Burt (1982) as "a coarse-grained body of calc-silicate in relatively pure carbonate formed by infiltration and diffusion of metasomatic fluids, containing exotic components" [mainly silica in reaction (2)]. Given that some calcite remains after completion of reaction (2), we conclude that the reaction is limited by the availability of silica. We were unable to find petrographic evidence for the volume gain inferred by reaction (2c), but we note that volume gain could have been accommodated within the shear zone and/or compensated by volume loss in the gneiss (see below).

The type I assemblage is subdivided in types Ia and Ib. Both represent *sensu stricto* carbonatites in that modal calcite exceeds 50%. Type Ia carbonatite contains >80% calcite and ~10% biotite. Biotite occurs as large euhedral crystals (Figs. 2f, 3h). Type Ib carbonatite contains over 50% calcite and up to 50% diopside + nepheline. Diopside and nepheline occur as variably corroded crystals (Fig. 3d, e). This spatial coupling of the corrosion of diopside/nepheline and the growth of biotite is presented by Hode Vuorinen and Skelton (2004) as evidence for the acquisition of these silicate minerals by mechanical/chemical assimilation and as a chemical by-product of the assimilation process.

Reaction progress (ξ)

In our study, we define the volumetric progress of reactions (1) and (2) ($\xi_{[1]}$ and $\xi_{[2]}$, respectively), by:

$$\left.\begin{aligned} \xi_{[1]} &= 1 - \frac{\sum x_j}{N} \\ \xi_{[2]} &= \frac{\sum x_k}{N} \end{aligned}\right\} \quad (3)$$

where the reactant minerals (j) for reaction (1) are biotite, oligoclase and quartz and the product mineral (k) for reaction (2) is wollastonite. We estimated $x_{\text{oligoclase}}$ by assuming that it covaried with $x_{\text{biotite}} + x_{\text{quartz}}$. N is the percentage of the rock which is involved in the reaction. Thus N = 78.4% for reaction (1) and $N = [100 - x_{\text{diopside}} - x_{\text{nepheline}}]$% for reaction (1). Reaction progress is represented in Fig. 5 by its moving average (ξ'), which (for the ith data point) is given by:

$$\xi' = \frac{2\xi_i + \xi_{i-1} + \xi_{i+1}}{4} \quad (4)$$

The reason for representing reaction progress by its moving average is to highlight variations that are sustained on a length scale, which is greater than the sample spacing (dm–m). This profile was used to position the types I and II mineral assemblage zones for comparison with stable isotope data (Fig. 5).

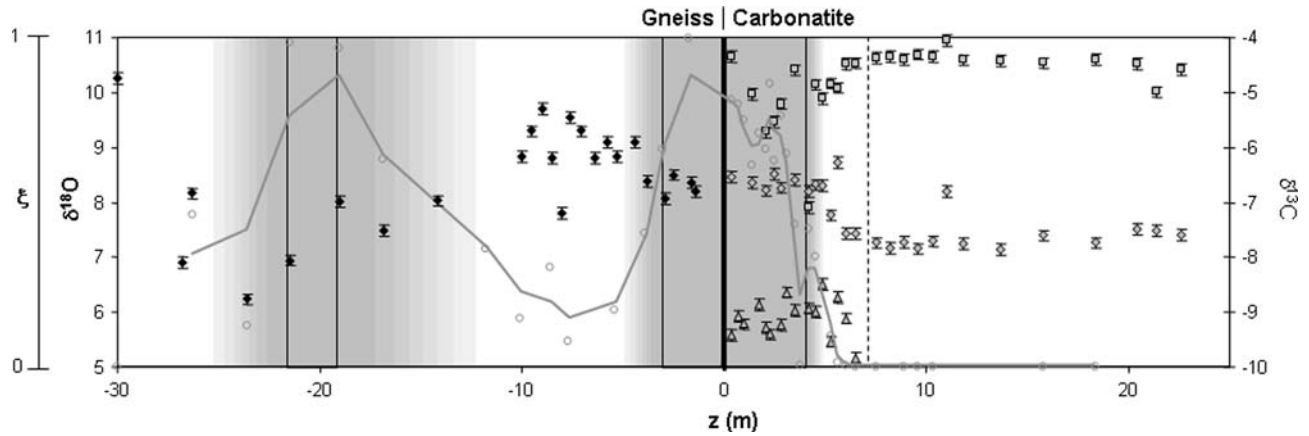

Fig. 5 Profile across the outcrop at Smedsgården showing δ^{18}O-feldspar (*black diamonds*), δ^{18}O-diopside (*grey triangles*), δ^{18}O-calcite (*grey diamonds*), δ^{13}C-calcite (*grey squares*), reaction progress [(*grey open circles*) and its moving average (*gray curve*, see (4a)]. The type I and II regions and the gneiss-carbonatite contact are shown. *Greyscale* intensity schematically represents the extent of metasomatism

Volume change

Finally, we were able to test whether the 3.9% volume loss in the gneiss [which is inferred by equation (1c)] could have accommodated the 1.6% volume gain in the carbonatite [which is inferred by equation (2c)] as follows:

For the gneiss and carbonatite, we calculated the total volume of reacted rock occupying a column of unit area, oriented perpendicular to the boundary surface at $z = 0$ m, by integrating reaction progress between this surface and the respective reaction front. For the gneiss, we calculated a total volume of 3.9 m^3 m^{-2}. The respective volume loss (–3.9%) is –0.15 m^3 m^{-2}. For the carbonatite, we calculated a total volume of 2.9 m^3 m^{-2}. The respective volume gain (+1.6%) is +0.05 m^3 m^{-2}. We can thus confirm that the volume loss in the gneiss could have accommodated the volume gain in the carbonatite. The additional volume loss in the gneiss could have been accommodated by deformation within the shear zone.

Isotopic evidence of fluid–rock interaction

δ^{18}O and δ^{13}C of calcite separates were measured wi-than on-line Kiel device equipped to an IRMS (Finnigan Mat 252) at the Department of Geology and Geochemistry, Stockholm University. The analyses were done on ~100 μg separates and reported using the conventional δ-notation with respect to V-PDB (δ^{13}C) and V-SMOW (δ^{18}O). Precision was better than ±0.1‰. δ^{18}O of feldspar and diopside separates were measured by a modification of the Sharp (1990) laser fluorination technique described by Macaulay et al. (2000) at the Scottish Universities Environmental Research Centre. Sample size was ca. 1 mg, and the fluorinating reagent was chlorine trifluoride. NBS28 quartz gives δ^{18}O = 9.6 ‰ V-SMOW by this method and precision is usually ±0.1 ‰ (1σ). Data are listed in Table 1.

In Fig. 5, δ^{18}O and δ^{13}C are plotted together with the progress of reactions (1) and (2) and the types I and II mineral assemblage zones. In the carbonatite, δ^{18}O and δ^{13}C were measured on calcite separates and δ^{18}O was measured on diopside separates. In the gneiss, δ^{18}O was measured on feldspar separates. Comparison of these plots and the mineral assemblage zonation yields the following observations:

- Calcite-δ^{18}O and δ^{13}C from the type I carbonatite are 7.3 ± 0.1‰ (n = 14) and –4.4 ± 0.2‰ (n = 15), respectively. These values fall within the ''primary carbonatite field'' of Taylor et al. (1967). Diopside-δ^{18}O from the type I carbonatite is 5.2 ± 0.1‰ (n = 1).
- Calcite-δ^{18}O and δ^{13}C from the type II carbonatite are 8.3 ± 0.2‰ (n = 11) and –5.2 ± 0.7‰ (n = 11), respectively. Diopside-δ^{18}O from the type II carbonatite is 5.9 ± 0.3‰ (n = 11).
- Feldspar-δ^{18}O from the type I gneiss is 9.0 ± 0.5‰ (n = 11). These values are reasonable for a rock of metasedimentary origin (cf. Taylor 1968). Feldspar-δ^{18}O from gneiss samples collected >1 km from the Alnö complex are 10.3 ± 0.8‰.
- Feldspar-δ^{18}O from the region of type II gneiss, which is adjacent to the shear zone, is 8.3 ± 0.2‰ (n = 5). Feldspar-δ^{18}O from the region of type II gneiss centred on the zone of Fe-veining is 7.4 ± 0.7‰ (n = 7).

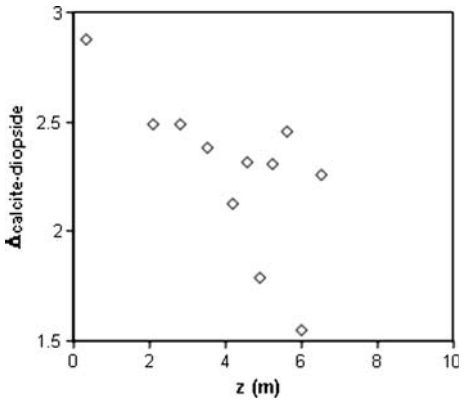

Fig. 6 Calcite–diopside isotopic fractionation factors plotted against distance from the shear zone ($z = 0$ m). At $z = 0$ m, $\Delta_{\text{calcite–diopside}} \approx 2.7‰$

Isotopic fractionation

Comparison between oxygen isotope data from mineral separates requires knowledge of inter-mineral fractionation factors at the temperature of interest. In the temperature range of carbonatite crystallisation (550–750°C, Haynes et al. 2003), calcite–feldspar oxygen isotope fractionation ($\Delta_{\text{calcite-feldspar}}$) ranges from 0.8–0.9‰ (at 550°C) to 0.5–0.6‰ (at 750°C) (Chiba et al. 1989; Hoffbauer et al. 1994) and calcite-diopside oxygen isotope fractionation ($\Delta_{\text{calcite-diopside}}$) ranges from 3.5‰ (at 550°C) to 2.3‰ (at 750°C) (Chiba et al. 1989). For post-magmatism temperatures ($T < 550$°C), $\Delta_{\text{calcite-feldspar}}$ is greater than 0.9‰ and $\Delta_{\text{calcite-diopside}}$ is greater than 3.5‰.

Calcite–diopside fractionation is plotted against distance in Fig. 6. This plot shows that $\Delta_{\text{calcite-diopside}}$ decreases from 2.7‰ adjacent to the shear zone to <2.0‰ in the type Ib carbonatite. This could be explained by chilling of the carbonatite margin to 660°C from ≥ 830°C in its interior. However, because this temperature range is probably too high for carbonatite crystallisation (Haynes et al. 2003) and because diopside was likely assimilated by (rather than crystallised from) the carbonatite liquid (Hode Vuorinen and Skelton 2004), we suggest an alternative hypothesis: that isotopic equilibrium between calcite and diopside is only approached at the carbonatite margin, where isotopic exchange is facilitated by fluid–rock interaction.

Comparison of $\Delta_{\text{calcite-diopside}}$ calculated from calcite- and diopside-δ^{18}O at the carbonatite margin with $\Delta_{\text{calcite-feldspar}}$ estimated from calcite-δ^{18}O (in the carbonatite) and feldspar-δ^{18}O (in the gneiss) yields a temperature estimate of 640°C, which is within the margin of error for both calculated/estimated fractionation factors. We thus interpret that equilibration of calcite-, diopside- and feldspar-δ^{18}O occurred within the metasomatised (type II) regions of the gneiss and carbonatite on either side of the shear zone at 640°C. We suggest that this was facilitated by fluid channelling caused by structural and reactive permeability enhancement within this region. This not only explains homogenization of δ^{18}O, but also coeval (?) metasomatism of both the gneiss and carbonatite. In contrast, variation in δ^{13}C between type II carbonatite samples was preserved. This is expressed by its higher standard deviation (±0.7‰) and can be explained by the lower volumetric fluid/solid partition coefficient (K_V) for carbon than for oxygen (see below). Finally, the lower δ^{18}O of the fluid which caused hematite veining can be explained by equilibration with carbonatite at lower temperatures or with alkaline rocks.

Reaction and isotope fronts

The metasomatised (type II) region is bounded by reaction and isotope fronts. Separating types I and II gneiss and on either side of the zone of hematite veining at $z = 23.6$ m, these fronts coincide (Fig. 7), whereas the reaction front which separates types I and

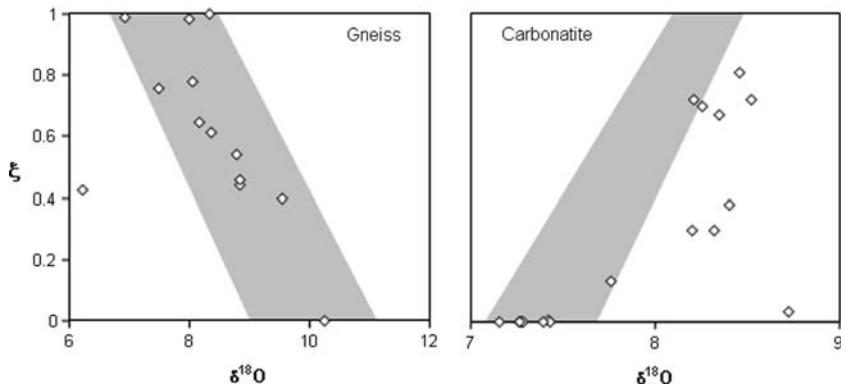

Fig. 7 Plots of ξ versus δ^{18}O for the gneiss and carbonatite. In the shaded regions, ξ covaries with δ^{18}O (i.e., the reaction and isotope fronts are spatially coincident)

II carbonatite lags behind the corresponding isotope fronts (Fig. 7). These are important observations, from which we can interpret the following:

- Fluid channelling occurs within the metasomatised (type II) region. In the gneiss, we suggest *reactive* permeability enhancement, which is consistent with the 3.9% volume reduction inferred by reaction (1c). In the carbonatite, we predict *mechanical* permeability enhancement, *which must be restricted to a narrow region immediately behind the reaction front* if reaction (2) proceeds with a 1.6% volume gain (see 2c).
- Fluid flow within these regions of enhanced permeability was dominantly layer-parallel with only a minor cross-layer component. This was oriented towards the carbonatite interior and caused the isotope fronts to propagate ''downstream'' of the reaction front.

Fluid channeling within the metasomatised (type II) region supports our hypothesis that wollastonite was produced by metasomatism of the carbonatite, rather than by igneous crystallization or metasomatism of the gneiss.

If local grain-scale equilibrium between fluid and calcite can be assumed and porosity (φ) is small, the cross-layer component of fluid transport towards the carbonatite interior can be described by the equation (e.g., Bear 1972):

$$K_{\mathrm{V}}\frac{\partial C_{\mathrm{f}}}{\partial t}+\omega\,\varphi\,\frac{\partial C_{\mathrm{f}}}{\partial z}+D_{\mathrm{f}}\,\varphi\,\tau\,\frac{\partial^2 C_{\mathrm{f}}}{\partial z^2}=0 \tag{5}$$

where C_{f} is the concentration of the reactant or isotopic species in the fluid, t is time, z is distance, ω is fluid velocity, D_{f} is diffusivity in the fluid, τ is tortuosity and K_{V} is the volumetric fluid/solid partition coefficient, which is given by:

$$K_{\mathrm{V}}=\begin{cases}\dfrac{C_{\mathrm{s}}\,\rho_s}{C_{\mathrm{f}}\,\rho_f}\text{(for isotopic transport)}\\[2ex]\dfrac{\left(C_{\mathrm{s},2}-C_{s,1}\right)\rho_s}{\left(C_{\mathrm{f},2}-C_{f,1}\right)\rho_f}\text{(for reactive transport)}\end{cases} \tag{6}$$

where C_{s} is the concentration of the reactant or isotopic species in the solid at position z, $C_{\mathrm{s},1}$ and $C_{\mathrm{s},2}$ are the respective concentrations of the reactant or isotopic species upstream and downstream of the geochemical front, and ρ_{f} and ρ_{s} are the respective fluid and solid densities. The solution of equation (5) for the boundary conditions:

$$\left.\begin{aligned}C_{\mathrm{s}}&=C_{\mathrm{s},1}\left(t=0,z<z_{\mathrm{p.b.}}\right)\\C_{\mathrm{s}}&=C_{\mathrm{s},2}\left(t=0,z>z_{\mathrm{p.b.}}\right)\end{aligned}\right\} \tag{7}$$

where $z_{\mathrm{p.b.}}$ is the position of a ''pinned boundary'' (see Bickle and Baker 1990) is given by (e.g., Lapidus and Amundson 1952):

$$\begin{aligned}\frac{C_{\mathrm{s}}-C_{\mathrm{s},2}}{C_{\mathrm{s},1}-C_{\mathrm{s},2}}=0.5\Bigg[&1+\mathrm{erf}\left(\frac{\left(\frac{\omega\varphi\cdot t}{K_{\mathrm{V}}}\right)-\left(z-z_{\mathrm{p.b.}}\right)}{2\sqrt{D_{\mathrm{f}}\varphi\tau\cdot t}}\right)\\&+\exp\left(\frac{\omega\varphi\cdot t\left(z-z_{\mathrm{p.b.}}\right)}{D_{\mathrm{f}}\varphi\tau\cdot t}\right)\\&\times\mathrm{erfc}\left(\frac{\left(\frac{\omega\varphi\cdot t}{K_{\mathrm{V}}}\right)+\left(z-z_{\mathrm{p.b.}}\right)}{2\sqrt{D_{\mathrm{f}}\varphi\tau\cdot t}}\right)\Bigg]\end{aligned} \tag{8}$$

Equation (8) expresses C_{s} as a function of z, $z_{\mathrm{p.b.}}$ and the transport parameters: $\omega\varphi\cdot t$ and $\sqrt{D_{\mathrm{f}}\varphi\tau\cdot t}$. Note that (1) $\omega\varphi$ = fluid velocity (ω) × fluid volume (φ) = volumetric fluid flux rate and $\omega\varphi\cdot t$ = fluid flux rate ($\omega\varphi$) × time (t) = time integrated volumetric fluid flux, and (2) $\sqrt{D_{\mathrm{f}}\varphi\tau\cdot t}$ is a characteristic length scale for diffusive transport. The boundary conditions (7) permit fluid transport downstream (towards the carbonatite interior) from a pinned boundary (near the contact between types I and II carbonatite). If $C_{\mathrm{s},1}$, $C_{\mathrm{s},2}$ and K_{V} can be determined, $\omega\varphi\cdot t$, $\sqrt{D_{\mathrm{f}}\varphi\tau\cdot t}$ and $z_{\mathrm{p.b.}}$ can be evaluated from the best fit of equation (8) to a plot of C_{s} against z.

In the following analysis, we evaluate $\omega\varphi\cdot t$, $\sqrt{D_{\mathrm{f}}\varphi\tau\cdot t}$ and $z_{\mathrm{p.b.}}$ for reaction progress (ξ), calcite-δ^{18}O and calcite-δ^{13}C. Diopside-δ^{18}O was excluded from this analysis because $C_{\mathrm{s},2}$ is unconstrained. Furthermore, based on calcite–diopside isotopic fractionation (Fig. 6), we conclude that isotopic equilibration between diopside and the fluid was slower than for calcite and that (for diopside) the assumption of fluid–solid local equilibrium was probably invalid.

K_{V} was evaluated for (1) the reaction and (2) the isotope (calcite-δ^{18}O and calcite-δ^{13}C) fronts as follows:

1. For the reaction front, K_{V} was estimated using (6). The initial and final concentrations of silica in the fluid ($C_{\mathrm{f},2}$ and $C_{\mathrm{f},1}$, respectively), were set to 0.0073 ± 0.0008 (T = 650°C, P = 0.2 GPa: Pak et al. 2003) and 0, respectively. The initial concentration of silica in the rock ($C_{\mathrm{s},1}$) was set to 0 and its final concentration ($C_{\mathrm{s},2}$) after production of 36 ± 12 volume% wollastonite was estimated to 0.19 ± 0.06. The fluid and solid densities were set

to 1 and 3 g cm^{-3}, respectively. This yielded K_V = 77 ± 35.

2. For oxygen and carbon, K_V was estimated using (5). We assumed a binary H_2O–CO_2 fluid and, for X_{CO_2} buffered by reaction (2), we calculated a value of 0.44 ± 0.01 at 640°C and 0.2 GPa using the computer program THERMOCALC (Holland and Powell 1998). That the fluid contains significant CO_2 is supported by the fluid inclusion study by Morogan and Lindblom (1995), but our estimate ignores the high salt content reported for some fluid inclusions by these authors. For oxygen and carbon, we estimated C_f = 0.82 ± 0.03 and 0.119 ± 0.004, respectively. We estimated C_s for a rock containing >80 volume% calcite and <20 volume% silicate phases (Fig. 4). Thus, for oxygen and carbon, we estimated $C_s \approx 0.49$ and 0.10, respectively. The fluid and solid densities were set to 1 and 2.75 g cm^{-3}, respectively. This yielded K_V = 1.65 ± 0.05 and 2.22 ± 0.07, respectively.

Next, we evaluated $\sqrt{D_f\varphi\tau \cdot t}$ and the position of the pinned boundary ($z_{p.b.}$) *for the reaction front only* for a range of preset values of $\omega\varphi$·t (from 0 to 6 m). We used the non-linear regression method provided with the computer program DATAFIT (Oakdale Engineering). For equations (8) rewritten in the form:

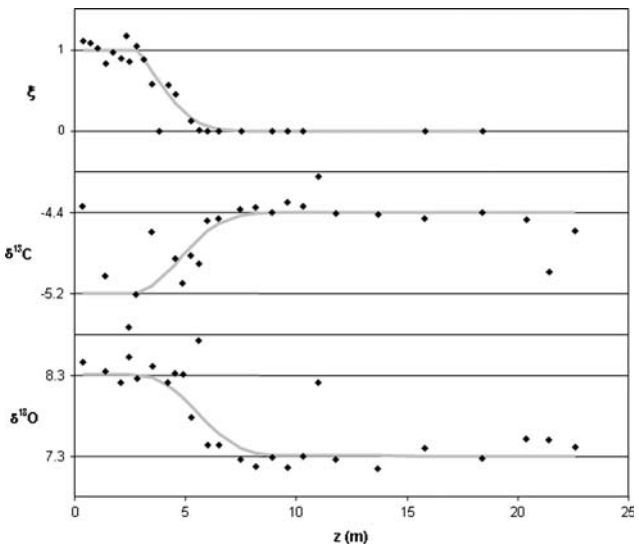

Fig. 8 Estimated R_a^2 (*dashed line*) and χ^2 (*solid line*) plotted against preset $\omega\varphi$ *t*. The best-fit is obtained for $\omega\varphi$ *t* = 4 m (i.e., maximum R_a^2 and minimum χ^2). Error envelope generated by propagation of the input errors for K_V

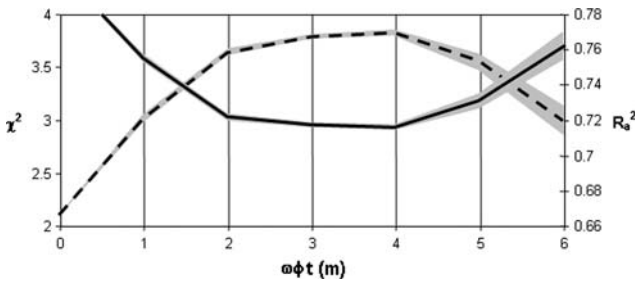

Fig. 9 Best-fit curves for (8) to reaction progress (ξ), calcite-$\delta^{13}C$ and calcite-$\delta^{18}O$. Parameterisations are: $\omega\phi \cdot$ *t* = 4 m, $\sqrt{D_f\varphi\tau \cdot t} = 1.5 \pm 0.5$ m, $z_{p.b.}$ = 2.8 ± 0.2 m, total χ^2 = 2.93 and average R_a^2 = 0.77

$$y = y\left(z; \omega\varphi \cdot t, \sqrt{D_f\varphi\tau \cdot t}, z_{p.b.}\right) \tag{9}$$

DATAFIT iteratively minimizes the merit function (χ^2):

$$\chi^2 = \sum_{i=1}^{N} \left[\frac{y_i - y\left(z_i; \omega\varphi \cdot t, \sqrt{D_f\varphi\tau \cdot t}, z_{p.b.}\right)}{\sigma_i}\right]^2 \tag{10}$$

where σ_i is the standard deviation of the *i*th data point. The adjusted coefficient of multiple determination (R_a^2: see "Appendix 2") was used to quantify goodness-of-fit.

Finally, we input the values of $\sqrt{D_f\varphi\tau \cdot t}$ and $z_{p.b.}$, which we obtained for each preset value of $\omega\varphi$·*t*, together with the appropriate value of K_V to evaluate the goodness-of-fit for each of the isotopic fronts.

The best-fit values of $\sqrt{D_f\varphi\tau \cdot t}$ and $z_{p.b.}$ for the reaction *and* isotope fronts are 1.5 ± 0.5 and 2.8 ± 0.2 m, respectively. These were obtained with $\omega\varphi$·*t* = 4 m and yielded *total* χ^2 = 2.93 ± 0.02 and *average* R_a^2 = 0.770 ± 0.001 (Figs. 8, 9; Table 3). We thus conclude that equation (8) gives a reasonable prediction of the observed spacing of the reaction and isotope fronts. This supports the validity of the assumption that local equilibrium between calcite and the pore fluid is maintained. We also tested two alternative scenarios: with pure diffusive transport (i.e., $\omega\varphi$·*t* = 0 m) and with the pinned boundary fixed to the shear zone ($z_{p.b.}$ = 0 m). Both alternative scenarios yielded poorer results: R_a^2 = 0.67 and 0.30, respectively.

The duration of fluid–rock interaction (*t*) can be evaluated from our estimate of $\sqrt{D_f\varphi\tau \cdot t}$. For $D_f \approx 10^{-7}$m^2 s^{-1} at 600°C (Krynicki et al. 1979), tortuosity, (τ) ≈ 0.7 ± 0.1 (estimated from thin-section images, assuming grain-edge flow) and $\varphi = 10^{-3}$–10^{-4} (Ferry and Dipple 1991), we estimate that the duration of fluid–rock interaction (*t*) is 10^2–10^4 years. This is a similar order-of-magnitude to the timescale for cooling

Table 3 Input and output parameters

Parameter	ξ	$\delta^{13}C$	$\delta^{18}O$	Total	Average
C_f		0.119 ± 0.004	0.82 ± 0.03		
C_s		0.10	0.49		
$C_{f,1}$	0				
$C_{f,2}$	0.0073 ± 0.0008				
$C_{s,1}$	0				
$C_{s,2}$	0.19 ± 0.06				
ρ_f	1.0 g cm^{-3}	1.0 g cm^{-3}	1.0 g cm^{-3}		
ρ_s	3.0 g cm^{-3}	2.7 g cm^{-3}	2.7 g cm^{-3}		
K_V	*77 ± 35*	*2.22 ± 0.07*	*1.65 ± 0.05*		
$\omega\ \varphi{\cdot}t = 0$					
$\sqrt{D_f\varphi\tau\cdot t}$	**0.5** ± **0.4** m	*0.5* m	*0.5* m		
$z_{p.b.}$	**3.7** ± **0.3** m	*3.7* m	*3.7* m		
χ^2	**0.30**	**2.66**	**1.46**	**4.42**	
R_a^2	**0.94**	**0.32**	**0.74**		**0.67**
$\omega\ \varphi{\cdot}t = 4$					
$\sqrt{D_f\varphi\tau\cdot t}$	**1.5** ± **0.5** m	*1.5* m	*1.5* m		
z p.b.	**2.8** ± **0.2** m	*2.8* m	*2.8* m		
χ^2	**0.18**	**2.13**	**0.63**	**2.93**	
R_a^2	**0.96**	**0.46**	**0.89**		**0.77**
$z_{p.b.} = 0$					
$\sqrt{D_f\varphi\tau\cdot t}$	**22** ± **3** m	*22* m	*22* m		
$\omega\ \varphi{\cdot}t$	**33** ± **1** m	*33* m	*33* m		
χ^2	**0.42**	**7.7**	**10.7**	**18.8**	
R_a^2	**0.91**	0	0		**0.30**

Input and output parameters for transport modelling for the three scenarios: $\omega\varphi{\cdot}t$ = 0 m (diffusion only), $\omega\varphi{\cdot}t$ = 4 m (best-fit solution for coupled advection and diffusion, see Fig. 8) and $z_{p.b.}$ = 0 m (pinned boundary fixed to the shear zone). Parameters used to estimate K_V are shown in normal text. Input parameters are shown in italic and output parameters are shown in bold

of the carbonatite dyke (cf. Jaeger 1968) and thus we speculate that fluid flow was thermally driven.

Conclusion

We conclude that fluid infiltration along the contact between carbonatite (containing/infiltrating partially assimilated ijolite) and gneiss at Smedsgården, Alnö occurred during (or not long after) emplacement of the carbonatite at an estimated temperature of 640°C. We calculate that the duration of this fluid-infiltration event was 10^2–10^4 years and conclude that it caused the following:

- Isotopic homogenization of the metasomatised region to 8.3 ± 0.2‰, which is consistent with the incoming fluid having equilibrated with a mixed gneiss + alkaline magma ± carbonatite source region.
- Metasomatism of the gneiss, by the reaction (1): biotite + quartz + oligoclase = albite + K-feldspar + arfvedsonite + aegirene – augite + H_2O, which requires that the incoming fluid added Na_2O, K_2O, CaO, MgO and FeO and that the outgoing fluid removed SiO_2. This is similar to ''fenitisation'' as defined by Brögger (1921) in that alkalis are added and silica is removed. We thus argue that extensive fenitisation occurs only within a few meters of the carbonatite (cf. Eckermann 1948; Kresten 1979, 1980; Morogan and Woolley 1988).
- Metasomatism of the carbonatite, by the reaction (2): calcite + SiO_2 = wollastonite + CO_2, which

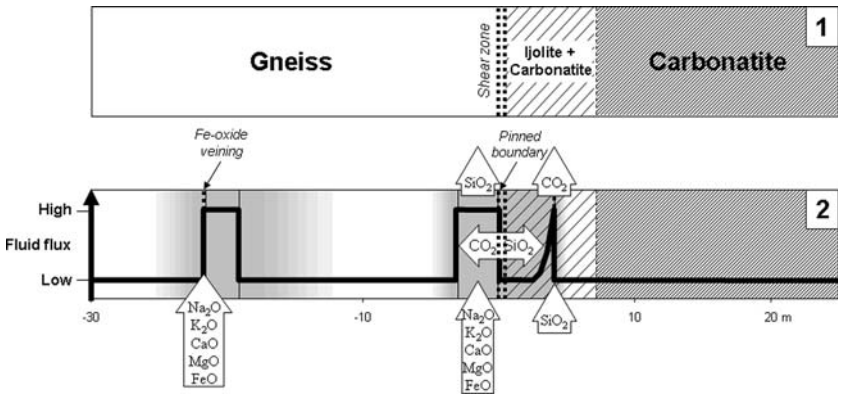

Fig. 10 Model showing Smedsgården profile before (1) and during and after (2) fluid–rock interaction

required that the incoming fluid added SiO_2. This conforms to the definition of skarning by Einaudi and Burt (1982).

We suggest that coupled reactive and structural weakening, initiated along the shear zone, caused the metasomatised region to widen. Fluids were channelled within the metasomatised gneiss and along a narrow region of enhanced permeability, located immediately behind the reaction front in the carbonatite. Continued reactive and isotopic transport from this region caused further propagation and broadening of reaction and isotope fronts from the metasomatised region and towards the carbonatite interior. Our interpretation is summarised in Fig. 10.

We further suggest that metasomatic reactions (1) and (2) are chemically coupled as follows: reaction (1) produces SiO_2 which is required for the forwards progress of reaction (2). Also, reaction (2) produces CO_2, which, together with salt in the fluid (Morogan and Lindblom 1995), will lower the activity of H_2O, thus favouring the forwards progress of reaction (1). It is further possible that reactions (1) and (2) are mechanically coupled in that the volume loss, inferred by reaction (1c), could accommodate the volume gain, inferred by reaction (2c).

We also note that further metasomatism and isotopic modification of the gneiss accompanied hematite veining. This was caused by infiltration of a second fluid either at lower temperature or from a different source region, perhaps with a higher proportion of alkaline rocks.

Finally, ''removal'' of the metasomatic overprint reveals gneiss (Feldspar-$\delta^{18}O = 9.0 \pm 0.5‰$) juxtaposed against carbonatite (Calcite-$\delta^{18}O = 7.3 \pm 0.1‰$, Calcite-$\delta^{13}C = -4.4 \pm 0.2‰$) along a shear zone (Fig. 10). The carbonatite contained partly assimilated ijolite minerals (nepheline + diopside), reactive by-products of the assimilation process (phlogopite). In this study, we show that wollastonite could have been added to the carbonatite by metasomatism. We thus conclude that the carbonatite at Smedsgården, Alnö was a relatively pure melt (or fluid?), which contained calcite + H_2O + CO_2 ±salt, but few or no silicate phases.

Acknowledgments This project was supported by Stockholm University and Stiftelsen Lars Hiertas Minne. Klara Hajnal is thanked for analytical work. Colin Graham is thanked for useful discussions about some of the ideas presented in this study. Tom Andersen, Rainer Abart and Ian Parsons are thanked for constructive input on earlier versions of this manuscript.

Appendix 1: Table of symbols, recurring in this manuscript

Symbol	Description	Units
C_f	Concentration of the tracer in the fluid at z	
C_s	Concentration of the tracer in the solid at z	
$C_{s,1}$, $C_{s,2}$	Concentrations of the tracer in the solid upstream and downstream of the front	
K_V	Fluid solid partition coefficient by volume	
ρ	Density	gcm^{-3}
T	Time	s
z	Distance	m
$z_{p.b.}$	Position of the pinned boundary	m
$X_{j\ (or\ k)}$	Modal% of reactant mineral j (or product mineral k)	
$nj\ (or\ k)$	Number of moles of reactant mineral j (or product mineral k) per unit volume of rock	$mol\ m^{-3}$
N_I	Metasomatic addition (positive) or subtraction (negative) of component I per unit volume of rock	$mol\ m^{-3}$
$[i]_{j\ (or\ k)}$	Molar proportion of component i in reactant mineral j (or product mineral k)	
N	Modal% of rock involved in the reaction	
ξ	Reaction progress	
φ	Porosity	
ω	Fluid velocity	$m\ s^{-1}$
$\omega\ \varphi$	Fluid flux rate	$m^3\ m^{-2}\ s^{-1}$
$\omega\varphi \cdot t$	Time-integrated volumetric fluid flux	$m^3\ \ m^{-2}$ (or m)
D_f	Diffusivity in the fluid	$m^2\ s^{-1}$
τ	Tortuosity	
$\sqrt{D_f \varphi \tau \cdot t}$	Characteristic length scale of diffusion	m

Appendix 2: Parameterisation of goodness-of-fit

The goodness-of-fit is parameterised by R_a^2. This is the adjusted coefficient of multiple determination, which is given by:

$$R^2 = 1 - \frac{\sum_{i=1}^{n} \left(y_i - y\left(z_i; \omega\varphi \cdot t, \sqrt{D_{\mathrm{f}}\varphi\tau \cdot t}, z_{\mathrm{p.b.}}\right)\right)^2}{\sum_{i=1}^{n} \left(y_i - \bar{y}\right)^2}$$

$$R_{\mathrm{a}}^2 = \frac{(n-1)R^2 - k}{n - 1 - k}$$

for equation (4) rewritten as (7), with k = number of regression parameters, n = number of data points and $\sum_{i=1}^{n} (y_i - \bar{y})^2$ = total variation of parameter y. R_{a}^2 is the fraction of the variance in y which is explained by the model, $y(z_{\mathrm{i}};\ \omega\varphi{\cdot}t,\ \sqrt{D_{\mathrm{f}}\varphi\tau \cdot t},\ z_{\mathrm{p.b.}})$ and can vary between 0 and 1.

References

Andersen T (1996) Sr, Nd and Pb isotopic data of the Alnö complex 22nd Nordic Geological Winter Meeting, Abstract, vol 11

Bailey DK (1974) Nephelinites and ijolites. In: Sörensen H (ed) The alkaline rocks. Wiley, New York, p 622

Bear J (1972) Dynamics of fluids in porous media. Elsevier, Amsterdam

Bickle MJ, Baker J (1990) Advective-diffusive transport of isotopic fronts: an example from Naxos, Greece. Earth Planet Sci Lett 97:78–93

Brögger (1921) Die Eruptivgesteine des Kristianiagebietes, IV. Das Fengebiet in Telemark, Norwegen Vidensk Selsk Skrift I, Mat-Naturv Klasse, 9

Chiba H, Chacko T, Clayton RN, Goldsmith JR (1989) Oxygen isotope fractionations involving diopside, forserite, magnetite and calcite: applications to geothermometry. Geochim Cosmochim Acta 53:2985–2995

Church AA, Jones AP (1995) Silicate-carbonate immiscibility at Oldoinyo Lenagi. J Petrol 36:869–889

Eckermann H (1948) The alkaline district of Alnö Island. Sver Geol Unders Ca 36:1–176

Einaudi MT, Burt DM (1982) Introduction; terminology, classification, and composition of skarn deposits. Econ Geol 77:745–754

Ferry JM, Dipple GM (1991) Fluid flow, mineral reactions, and metasomatism. Geology 19:211–214

Gresens RL (1967) Composition-volume relationships of metasomatism. Chem Geol 2:47–65

Haynes EA, Moecher DP, Spicuzza MJ (2003) Oxygen isotope composition of carbonates, silicates, and oxides in selected carbonatites; constraints on crystallization temperatures of carbonatite magmas. Chem Geol 193:43–57

Hode Vuorinen J, Skelton ADL (2004) Origin of silicate minerals in carbonatites—in situ crystallisation or wall rock contamination? Terra Nova 16:210–215

Hode Vuorinen J, Hålenius U, Whitehouse MJ, Mansfeld J, Skelton ADL (2005) Compositional variations (major and trace elements) of clinopyroxene and Ti-andradite from pyroxenite, ijolite and nepheline syenite, Alnö Island, Sweden. Lithos 81:55–77

Hoffbauer R, Hoernes S, Fiorentini E (1994) Oxygen isotope thermometry based on a refined increment method and its application to granulite–grade rocks from Sri Lanka. In: Raith M, Hoernes S (eds), Tectonic, metamorphic and isotopic evolution of deep crustal rocks, with special emphasis on Sri Lanka. Precambrian Res 66:199–220

Holland TJB, Powell R (1998) An internally consistent thermodynamic dataset for phases of petrological interest. J Metamorph Geol 16:309–344

Jaeger JC (1968) Cooling and solidification of igneous rocks. In: Hess HH, Poldervaart A (eds), Basalts, the poldervaart treatise on rocks of basaltic composition. Wiley, New York, pp 503–537

Kramm U (1994) Isotope evidence for ijolite formation by fenitization: Sr–Nd data of ijolites from the type locality Iivaara. Finl Contrib Mineral Petrol 115:279–286

Kresten P (1979) The Alnö complex: discussion of the main features, bibliography and excursion guide Nordic Carbonatite Symposium, pp 67

Kresten P (1980) The Alnö complex; tectonics of dyke emplacement. Lithos 13:153–158

Kresten P, Morogan V (1986) Fenitization at the Fen complex, southern Norway. Lithos 19:27–42

Krynicki K, Green CD, Sawyer DW (1979) Pressure and temperature dependence of self-diffusion in water. Faraday Discuss Chem Soc 66:199–208

Lapidus L, Amundson NR (1952) Mathematics of adsorption in beds. IV. The effect of longitudinal diffusion in ion exchange and chromatographic columns. J Phys Chem 56:984–998

Macaulay CI, Fallick AE, Haszeldine RS, Graham CM (2000) Methods of laser-based stable isotope measurement applied to diagenetic cements and hydrocarbon reservoir quality. Clay Minerals 35:313–322

Morogan V, Lindblom S (1995) Volatiles associated with the alkaline—carbonatite magmatism at Alnö, Sweden: a study of fluid and solid inclusions in minerals from the Långarsholmen ring complex. Contrib Mineral Petrol 122:262–274

Morogan V, Woolley AR (1988) Fenitization at the Alnö carbonatite complex, Sweden: distribution, mineralogy and genesis. Contrib Mineral Petrol 100:169–182

Pak TM, Hauzenberger CA, Baumgartner LP (2003) Solubility of the assemblage albite+K-feldspar+andalusite+quartz in supercritical aqueous chloride solutions at 650 degrees C and 2 kbar. Chem Geol 200:377–393

Plas L van der, Tobi AC (1965) A chart for judging the reliability of point counting results. Am J Sci 263:87–90

Sharp ZD (1990) A laser-based microanalytical method for the in situ determination of oxygen isotope ratios in silicates and oxides. Geochim Cosmochim Acta 54:811–822

Sindern S, Kramm U (2000) Volume characteristics and element transfer of fenite aureoles: a case study from the Iivaara alkaline complex. Lithos 51:75–93

Sokolova NT, Khodakovskiy IL (1977) The mobility of aluminium in hydrothermal systems. Geochem Int 14:105–112

Taylor HP (1968) The oxygen isotope geochemistry of igneous rocks. Contrib Mineral Petrol 19:1–71

Taylor HP, Frechen J, Degens RT (1967) Oxygen and carbon isotope studies of carbonatites from the Laacher See district, West Germany, and the Alnö district, Sweden. Geochim Cosmochim Acta 31:407–430

Verschure RH, Maijer C (2005) A new Rb–Sr isotopic parameter for metasomatism, Δt, and its application in a study of plurifenitized gneisses around the Fen ring complex, South Norway. NGU Bull 445:45–71